Biogeosciences Discuss., 8, 4331–4357, 2011
www.biogeosciences-discuss.net/8/4331/2011/
doi:10.5194/bgd-8-4331-2011

Biogeosciences Discussions

The variability of radiative balance elements and air temperature on the Asian region of Russia

E. V. Kharyutkina, I. I. Ippolitov, and S. V. Loginov

Institute of Monitoring of Climatic and Ecological Systems, Academichesky ave, Tomsk, 10/3, SB RAS 634055, Russia

Received: 17 March 2011 – Accepted: 11 April 2011 – Published: 4 May 2011

Correspondence to: S. V. Loginov (ceo@imces.ru)

Published by Copernicus Publications on behalf of the European Geosciences Union.

Abstract

The variability of spatial-temporal distribution of temperature and radiative and heat balances components is investigated for the Asian territory of Russia (45–80° N, 60–180° E) using JRA-25, NCEP/DOE AMIP reanalysis data and observational data for the period of current global warming 1979–2008. It is shown that since the beginning of 90s of XX century the increase of back earth-atmosphere short-wave radiation is observed. Such tendency is in conformity with the cloud cover dynamics and downward short-wave radiation at the surface. Annual averaged radiative balance values at the top are negative; it is consistent with negative annual averaged air temperature, averaged over territory. The downward trend of radiative balance is the most obvious after the beginning of 90s of XX century.

1 Introduction

Radiation balance elements of the atmosphere, as well as sensible and latent heat fluxes between atmosphere and underlying surface play an important role in the weather and climate formation. Significant contribution to the study of these characteristics, which are the part of the earth's surface heat balance, was made by Budyko (1958). Heat transfer for different types of landscapes was studied by Pavlov (1980). Current constructions of the global energy and radiative balance are based on the analysis of assimilated data, satellite estimates of global radiant energy and turbulent heat over oceans, and/or the hybrid approach of in-situ and satellite measurements (Da Silva et al., 1994; Trenberth and Solomon, 1994; Rossow and Zhang, 1995; Trenberth and Stepaniak, 2004). The irradiative aspects have been explored in several studies by Zhang et al. (2004, 2006, 2007), based on International Satellite Cloud Climatology Project (ISCCP) cloud data and other data in an advanced irradiative code. In addition, estimates of surface radiation budgets have been given by Gupta et al. (1999) and used by Smith et al. (2002) and Wilber et al. (2006). These are based

BGD
8, 4331–4357, 2011

on earlier ISCCP data and reanalysis databases (Liu et al., 2005; Jimener et al., 2009) such as the NCEP/NCAR, NCEP AMIP/DOE, ERA40, and JRA-25.

Liu et al. (2005) have estimated different surface irradiative flux data sets in the Arctic Ocean, focusing on high temporal resolution at both the local and regional scales. The following atmospheric parameters were examined: the surface temperature, surface downward shortwave irradiative fluxes and surface downward longwave irradiative fluxes from two satellite based products (CASPR – Cloud and Surface Parameter Retrieval and ISCCP-FD is International Satellite Cloud Climatology Project), and two numerical weather prediction reanalysis (NCEP AMIP/DOE and ERA-40). The satellite-based products provide more accurate surface downward shortwave irradiative fluxes relative to the reanalysis, because the satellite-based products have better cloud properties than the reanalysis. The downward solar irradiative fluxes of ISCCP-FD, NCEP AMIP/DOE and ERA-40 show similar spatial variability, while the downward longwave irradiative fluxes of CASPR, NCAP AMIP/DOE and ERA-40 show similar spatial variability.

Serreze et al. (2007) synthesize a variety of atmospheric and oceanic data to examine the large-scale energy budget of the Arctic. Assessment of the atmospheric budget relies primarily on the ERA-40 and NCAR reanalysis. The seasonal cycles of vertically integrated atmospheric energy storage and the convergence of energy transport from ERA-40, as evaluated for the polar cap, in general, compare well with realizations from the NCAR. However, downward shortwave radiation at the top of atmosphere, as compared with satellite data, and the net surface flux, contribute to large energy budget residuals in ERA-40.

Estimation of sensible heat flux variability from the types of relief was executed by Foken (2008). The available energy, i.e. the sum of the net radiation and the ground heat flux, was found in most cases to be larger than the sum of the turbulent fluxes of sensible and latent heat. It is shown that an incorrect account of relief main type sizes may lead to a substantial change (including change sign) of turbulent heat flux estimation.

BGD
8, 4331–4357, 2011

Studies of radiation fluxes and sensible and latent heat fluxes are carried out by instrumental methods (Beyrich et al., 2006; Beyrich and Mengelkamp, 2006), calculations based on mathematical models (Heinemann and Kerschgens, 2006; Heret et al., 2006). Heinemann and Kerschgens (2005) tested the performance of different area-averaging methods for the turbulent surface fluxes for the LITFASS area, named aggregation, mosaic and tile methods. For one tile method (station-tile), the experimental setup of the surface energy balance stations of the LITFASS experiment was investigated. Two different simulation types are considered: (1) realistic topography and idealized synoptic forcing; (2) realistic topography and realistic synoptic forcing for LITFASS cases. The aggregation method yields generally higher errors than the mosaic method, which even increase for higher wind speeds. The main reason is the strong surface heterogeneity associated with the lakes and forests in the LITFASS area.

Experimental studies of radiation and turbulent heat flux in the atmospheric surface layer for summer conditions (August, 1981) carried out in the dry steppes of northern Kazakhstan by Eliseev et al. (2002). It is used opto-acoustic method in the long and short ranges. Studies of diurnal variations of radiation balance, an effective longwave irradiation and turbulent heat flux showed that the irradiative heat flux is largely compensated by the turbulent, as in the irradiative heating, and during a significant irradiative cooling. Only at night the turbulent heat flux was several times smaller than the radiation. The obtained results are important for research in arid zones.

Thus, any identified patterns of radiation can be subsequently used to explore potential relationships between surface energy budget and atmospheric circulation or other atmospheric parameters. In addition, identifying regions with common radiation variability and trends may be valuable in understanding of driving physical processes.

To achieve this aim, statistical methods that include both simple approaches and multivariate techniques are very useful tools. In particular, the use of factor analysis (FA) allows to define, in an objective way, geographical areas with common temporal variability of a specific climatological variable. Such an objective grouping of geographical places, based on the temporal co-variability of a specific parameter, is very useful

BGD
8, 4331–4357, 2011

as in this way of single time-series as representative for the whole area. Moreover, it can elucidate physical processes responsible for these correlations and reveal possible spatial patterns. For this reason, FA has been widely used in climatological studies, applied to meteorological parameters (Barnston and Livezey, 1987). On the contrary, the application of multivariate techniques on solar radiation is rather limited. Wilber et al. (2006) applied principal component analysis (PCA) to examine the annual cycle surface solar radiation. The major part of the variation is simply due to the variation of the insolation at the top of the atmosphere, especially for the first term, which describes 92.4 % of the variance for the downward shortwave flux. However, for the second term, which describes 4.1 % of the variance, the effect of clouds is quite important and the effect of clouds dominates the third term, which describes 2.4 % of the variance. To a large degree the second and the third terms are due to the response of clouds to the annual cycle of solar forcing. For net shortwave flux at the surface, similar variances are described by each term. The regional values of the EOFs are related to climate classes, thereby defining the range of annual cycles of shortwave radiation for each climate class.

Issues relevant to achieving an accuracy of better than 10 $W\,m^{-2}$ on 250-km scales for monthly means in the atmospheric energy balance are explored from the standpoint of the formulation and computational procedures using reanalysis data. In study (Badescu, 2008) linear relationship between daily global solar irradiation at ground level and cloudiness, maximum and minimum temperature by observational data was used. Calculation accuracy for the territory of Romania was 20 %. Among the output parameters of the reanalysis the information on radiation fluxes and the latent and sensible heat fluxes at the grid nodes covering the entire globe is contained, and the time series duration allows to investigate not only the interannual, but also decadal variability.

The purpose of this study is to investigate the spatial and temporal variability of the irradiative and heat balance of underlying surface over the Asian territory of Russia (ATR) in the period of modern global warming 1979–2008.

BGD
8, 4331–4357, 2011

2 Data and methods of analysis

To understand the spatial and temporal variability of surface temperature and its relation to elements of heat balance multivariate statistical techniques were used. The monthly averaged data of temperature, solar radiation were calculated from NCEP AMIP/DOE and JRA-25 reanalysis data. For temperature validation observational data from 454 stations were used over ATR and northern parts of Kazakhstan, Mongolia and China (Distribution data center NOAA, ftp://ftp.cdc.noaa.gov). Including stations of Kazakhstan, Mongolia and China was necessary for correct presentation of meteorological fields over the southern boundary of ATR. Satellite data and observational data from actinometrical stations were used for validation of solar radiation.

As the initial data JRA-25 data were used (the long-term reanalysis cooperative research project carried out by the Japan Meteorological Agency (JMA) and the Central Research Institute of Electric Power Industry CRIEPI, http://jra.kishou.go.jp/JRA-25/index_en.html). The data presented in the nodes of a regular latitude-longitude grid of $1.25^{\circ} \times 1.25^{\circ}$ at 23 isobaric levels from 1000 to 0.4 hPa with 6-h temporal resolution. To derive estimates, which characterize the spatial distribution of some quantity x over the territory, its correction on the latitudinal dependence (because of northward mesh decrease) was made: calculated values were multiplied by coefficient, which equal to contemporary areas ratio. Then, distribution function $F_x(x)$ was construct for the resulting sample. Sample size was ~2100 nodes. Median and interquartile scale sample was estimated by the empirical distribution function. Then to assess the correlation we used time series of average sample values, which were determined in such way. Correlation estimates, trends of the parameters and their standard errors σ_{tr} with level of 0.95 were carried out by generally accepted method (Ippolitov et al., 2008).

BGD
8, 4331–4357, 2011

3 Temperature field variability over Asian territory of Russia

According to IV IPCC Report (2007), linear trend of air surface global temperature for the period of 1906–2005 is 0.074 °C/decade, this value has significant increased during last several decades. Global temperature trend value by Assesment report on climate change and its consequences in Russian Federation (2008) was 0.18 °C/decade, and for temperature, averaged by the territory of Russia, trend value was 0.43 °C/decade. Spatial and temporal variability of temperature field for period 1976–2005 over Asian territory of Russia is investigated by Ippolitov et al. (2008). Obtained in this study average temperature and trend values, averaged by the territory, for every calendar months and for a year in general are presented in Table 1.

From the Table 1 it follows, that for the period of 1976–2005 the Asian territory of Russia was warmed by more than 1 °C. High positive statistically significant temperature trends are revealed in March, May, June, July, August and October. It is in a good agreement with spread statements in literature, that maximal trend values of warming in middle and high latitudes are observed in winter and spring months.

Over Asian territory of Russia temperature field variability is also characterized by significant spatial inhomogeneity. Distribution of air temperature trends (by observational data) for January and July is presented in Fig. 1.

In January there are differently directed processes over ATR (Fig. 1a). The process of warming is revealed over the central part of Siberia and along seaside, the process of cooling – over West Siberia and Chukotka, and warming is observed over 60 % of the territory. Probability density function of trend values, calculated by grid nodes $1^\circ \times 1^\circ$, is multimode and has a wide range of trend values from −1.5 °C/decade to +1.5 °C/decade. Trend value, averaged by the territory, is 0.27 °C/decade with standard deviation $\sigma_{tr} = 0.84$ °C/decade and it is not statistically significant.

In July (Fig. 1b) the warming is observed over 90 % of the territory, local centers of negative trends are revealed only in West Siberia. Probability trend distribution has one mode with average value 0.46 °C/decade and standard deviation $\sigma_{tr} = 0.29$°/decade. In

BGD
8, 4331–4357, 2011

general, in annual variability over the central part of Siberia the process of warming prevails, and over West Siberia the processes of warming alternate with the processes of cooling.

Annual averaged temperature values and trends, calculated for the period of 1979–2008 over ATR (global time series in JRA-25 have been started since 1979) are also shown in Table 1. From the comparison of contemporary values by observational data and JRA-25 (Table 1) it follows, that average temperatures and their trends are higher in reanalysis data, however, reanalysis data save a qualitative true imagination of temperature field variability. Correlation coefficient of annual averaged time series for 1979–2005 was 0.95. To maintain unified data format for all derived values, further for regression model definition we will use temperature field characteristics, calculated by JRA-25 reanalysis data.

4 Radiation and heat balance fluxes at the earth's surface and the variability of cloud cover

Cloudiness, as well as surface albedo, plays an important role in the energy balance of the Earth. Clouds contribute to the heating of the earth's surface due to the reradiated infrared radiation toward the earth's surface. On the other hand, clouds efficiently reflect downward solar radiation and contribute to cooling the climate system. At the present time it is considered that cloud cover weakly cools the climate, while high level clouds contribute to the increasing of greenhouse effect and low clouds – to cooling of the climate system (Chernokulsky et al., 2010).

Validation of downward shortwave radiation, based on network observations of actinometrical stations in Western Siberia was carried out by the method described in (Ippolitov et al., 2009). It is found that radiation unit in JRA reanalysis data, like radiation unit in reanalysis data NCEP/DOE AMIP-II, impartial characterizes the distribution of total radiation over Western Siberia, including mountain regions, although the annual averaged values of total radiation derived by reanalysis JRA should be reduced by 10–15 %. Validation of data JRA and other reanalyses of the total cloud cover were

BGD
8, 4331–4357, 2011

made in paper by Chernokulsky et al. (2010). It is shown that if global annual averaged cloudiness value for the Northern Hemisphere is 0.55, according to observational data, then the similar value by JRA reanalysis data is equal to 0.44, and the maximal coincidence with observational data is observed for ERA-40. Annual variations of cloud cover, constructed by JRA reanalysis, are also characterized by low values.

For ATR we compared the total cloudiness values by NCEP/DOE AMIP (http://www.esrl.noaa.gov/psd/data/gridded/data.ncep.reanalysis2.html) and JRA-25. The comparison showed that the time series related to the interval 1979–2008 are close to each other, the magnitude of discrepancy between time series of monthly averaged values is 1.5 %, and the difference of annual averaged values is 0.5 %.

For the following calculations both reanalysis were used, where symbols in superscript "J" and "N" indicate values, calculated by JRA-25 and NCEP/DOE AMIP, respectively.

Heat balance equation at the surface is:

$$B_S = Q_{\downarrow S} - Q_{\uparrow S} + L_{\downarrow S} - L_{\uparrow S} - LE - P - G, \quad (1)$$

here $Q_{\downarrow S}$ – downward short-wave radiation at the surface, $Q_{\uparrow S}$ – upward short-wave radiation at the surface, $L_{\downarrow S}$ – downward longwave radiation at the surface, $L_{\uparrow S}$ – upward longwave radiation at the surface, LE – latent heat, P – sensible heat, G – heat flux in the ground. Signs before LE, P and G depend on heat flux direction. Positive turbulent fluxes are directed away from the earth surface whilst positive net radiation is directed towards the earth surface.

From the analysis of TC and $Q_{\downarrow S}$ variability over ATR (Fig. 2) it follows that for JRA-25 and NCEP/DOE AMIP reanalysis datasets in subinterval 1979–1992 the decreasing of total cloudiness and the corresponding growth of downward short-wave radiation at the surface are observed. In the second subinterval 1992–2008 the situation is reverse. Estimates of total cloudiness changes over ATR by observational data at meteorological stations are made by Khlebnikova et al. (2009). It was found there that for the second half of XX century the total cloudiness trend over ATR is positive and

BGD
8, 4331–4357, 2011

equal to 0.04 % per 10 yr, but for the interval 1976 to 2005 trend is negative and equal to −0.05 %/decade. There is a certain agreement between these data and JRA, shown in Fig. 2, because, in general, linear trend for the period of 1979–2008 is also negative and equal to −0.02 %/decade.

Such temporal variability separation of downward short-wave solar radiation $Q_{\downarrow S}$ is also observed for interannual variability of zonally averaged values $Q_{\downarrow S}$ over ATR and Northern Hemisphere, especially from 50° to 60° N (Fig. 3a). Similar tendency is observed for zone from 60° to 70° N (not presented). Observational data at actinometrical stations in Siberia are in a good agreement with reanalysis data: majority of stations are also characterized by two subintervals in $Q_{\downarrow S}$ variability.

For instance, temporal variability for one of the stations is presented in Fig. 3b.

Tendency of downward short-wave solar radiation decrease was revealed by satellite data for the period of 1983–2005 (http://eosweb.larc.nasa.gov).

Table 2 shows the monthly averaged values of TC and $Q_{\downarrow S}$ over ATR with their standard deviation. The annual averaged long-term cloud cover is 53 %. The maximum value is 61 % in November and the minimum is 45 % in July. The maximum variability of cloud cover corresponds to the cold season.

The annual averaged value of short-wave downward solar radiation at the surface was 128 $W m^{-2}$ with maximum value of 269.5 $W m^{-2}$ in July and minimum value of 7 $W m^{-2}$ in December. The maximum of short-wave flux variability was also in cool season of year.

The spatial distribution of trend values of the upward longwave radiation $L_{\uparrow\infty}$ at the top and the downward solar radiation $Q_{\downarrow S}$ at the surface are similar. The decreasing of $Q_{\downarrow S}$ is observed in the central and northern part of ATR, while the increasing – in the southern part of the territory. Also $L_{\downarrow S}$ at the surface, $Q_{\downarrow\infty}$ at the top and the total clouds TC have the similar spatial distribution and the opposite behavior is observed for $L_{\uparrow\infty}$ at the top and $Q_{\downarrow S}$ at the surface. Spatial distributions of downward shortwave radiation at the surface $Q_{\downarrow S}$ and effective radiation E_{eff} also have anticorrelation with cloudiness variability (Fig. 4).

BGD
8, 4331–4357, 2011

It is more evident in July over West Siberia, Buryatia and Yakutia. In January $Q_{\downarrow S}$ variability is not significant, and effective radiation variation is mainly connected with cloudiness variability. There are some regions, which have both correlation and anticorrelation with cloudiness, for instance, Chukotka. Probably, it is connected with advection variability of moist air from the Pacific Ocean.

The results of our analysis of changes in the cloudiness structure have shown that, in general, for the period of under study over ATR the following tendency was observed: the contribution of high level clouds was increased (15 %), of middle level clouds was slightly decreased (1 %), and most markedly decreasing was observed for the part of low level clouds (20 %).

5 The spatial and temporal variability of latent and sensible heat fluxes

Heat exchange between surface and atmosphere takes place through longwave radiation fluxes, and sensible and latent heat fluxes. In temporal dynamics of the effective radiation $E_{\text{eff}} = L_{\uparrow S} - L_{\downarrow S}$ two periods with the change of gradient in the beginning of 90th are distinguished. In the first interval the effective radiation increased with the rate of 1.96 W m^{-2}/decade, while in the second one it was decreased with the rate of -0.13 W m^{-2}/decade.

In winter it is observed mainly zonal distribution with the largest values in the south of the territory. Several local minima occurred along the north part of Pacific coast and over the northern part of Western Siberia. The positive trend of the effective radiation is, in general, typical for the summer period and it is observed in the southern part of Eastern Siberia. This coincides with the region of the total clouds decreasing.

For surface air sensible and latent heat fluxes can be calculated as (Budyko, 1958):

$$P = \rho c_p D(T_S - T), \quad LE = \rho D(q_S - q), \tag{2}$$

here ρ is air density, c_p is air heat capacity at a constant pressure, D is the integral characteristic of the vertical turbulent transfer conditions between surface and atmosphere,

BGD
8, 4331–4357, 2011

T_s is surface temperature, T is surface temperature at 2 m, q_s, q are air specific humidity at temperatures T_s and T, respectively. The interval 1990–1996 is also marked out in the fluxes temporal dynamics. It is characterized by amplitude decreasing of anomalies. The wavelet spectrum analysis of monthly averaged time series of *LE* and *P* have shown that changes occur in the periodicities with scale less than five years. The monthly averaged values of *LE* and *P* over the ATR region with their standard deviation are shown in Table 2.

The latent heat *LE* trend, in general, is positive, and only 20 % of the territory are in the negative value area. The variability of *LE* is weak in the winter months, from April, the latent heat flux is increased over the south of Western and Eastern Siberia, as well as over Far East. From June negative trend is observed over the south of Western Siberia, positive – over the central and southern part of Eastern Siberia and Far East. In general the conformity of *LE* spatial distribution with cloud field is marked. We could not explain this negative trend by difference between trends of specific humidity q_s and q at the appropriate height.

Negative tendency prevails in the change of sensible heat flux *P*. This is due to a lower rate of temperature growth T_s, than T at height of 2 m. This conclusion is based on the comparison of temperature linear trends at appropriate vertical levels. It is confirmed by the analysis of JRA values, as well as observational data at stations (for example, in March at the Aleksandrovskoe (60°26′ N, 77°52′ E) −0.07 °C/decade, at Pudino (57°32′ N, 79°22′ E) −0.28 °C/decade, and at Barabinsk (55°22′ N, 78°24′ E) −0.22 °C/decade). In summer the two times increasing of σ is observed as for *P*, as its trend; it indicates that there are several areas with the processes occurring at different rates over ATR. Before summer the magnitudes of flux decreases over the territory of Western Siberia and increases over the Eastern Siberia. In summer the situation is opposite.

BGD
8, 4331–4357, 2011

6 Regression analysis of surface temperature variability versus heat balance components

For the determination of cloudiness influence on the temperature variability we used a regression model, which relates surface temperature anomalies δT with short-wave radiation anomalies δQ_n, $Q_n = Q_{\downarrow S} - Q_{\uparrow S}$, longwave radiation anomalies δE_{eff}, calculated for clear sky, anomalies of latent, sensibility heat, heat flux in the ground δE_g, $E_g = LE + P + G$, and with cloudiness anomalies δTC:

$$\delta T = \beta_1 \delta Q_n + \beta_2 \delta E_{\text{eff}} + \beta_3 \delta E_g + \beta_4 \delta \text{TC}, \quad (3)$$

The addition of the total cloud to predictors allows to increase the contribution of describable regression R^2 in general by 0.06, and for February and December – by 0.15 (Table 3), in that time the variability of R^2 was decreased in general by 0.02. Such regression analysis (Eq. 3) was carried out using NCEP/DOE AMIP reanalysis data, where we have found that determination coefficient is less by 15 % than that, calculated by JRA-25. We also investigated two subintervals, revealed in temporal variability of parameters of under study. It was obtained that the contribution of describable regression R^2 for each separate subintervals (1979–1992 and 1992–2008) is higher than R^2 for the whole period by 0.14. The value of R^2 slightly varies within a year: for the first subinterval – from 0.76 to 0.9; for the second subinterval – from 0.69 to 0.87.

It is seen from the Fig. 5., that the regions with high closeness of relation ($R^2 > 0.8$ on Cheddock scale, red color), and correspondingly with high level of prediction, are observed over coastal regions of Pacific ocean and over the northern part of West Siberia. In winter, with very high relation ($R^2 > 0.9$ on Cheddock scale) are zonally extended and located in the central part of Western and Eastern Siberia. The coastal regions of Arctic ocean are characterized, as a rule, weak relation ($R^2 < 0.3$, blue color). In summer months the relation in the central part of ATR becomes weaker, but for coastal regions the increasing of the contribution of describable dispersion is observed. In spring and autumn there are local zones with high closeness of relation mainly in the central and northern parts of ATR (Fig. 6).

BGD
8, 4331–4357, 2011

The contribution of each predictor in the regression analysis to the total variability of air temperature was calculated. In January, the largest contribution belongs to the effective radiation, i.e. to the balance of long-wave radiation (Table 4).

7 Conclusions

Regional variations of solar radiation flux obtained by reanalysis data are mainly conformed to total cloudiness and air temperature changes. In general, anomalies of short-wave and longwave radiation play a major role in the air temperature variability during the whole year.

From the beginning of 90s of XX century the growth of solar radiation, reflected by earth's atmosphere is observed. This growth coincides with cloud cover dynamics and downward short-wave solar radiation coming to the surface. Annual averaged radiative balance values at the top are negative, and values of annual average air temperature, averaged by the territory, are also negative. Hence, in spite of slight decreasing of radiative balance ($\sim 2\,\mathrm{W\,m^{-2}}$), we can suppose that the tendency of regional climatic system cooling is possible; it can decelerate the growth of air temperature at the surface.

The variability of cloudiness in the summer time is in a good agreement with the variability of Atlantic Ocean surface temperature in the region of Newfoundland energy active zone. It allows to suppose that latent heat flux change in the ocean, which linearly depend on ocean surface temperature, influences on the process of cloudiness formation over the Asian territory of Russia.

Such research has shown that for several regions of ATR it is possible to predict air surface temperature variability using heat balance elements at the earth surface. For future investigation to get more accurate regression model, circulation processes in troposphere should be taken into account.

BGD
8, 4331–4357, 2011

Acknowledgements. This work was supported by FPP No. 02.740.11.0738 and SB RAS VII.63.1.1.

References

Badescu, V. (Ed.): Modeling Solar Radiation at the Earth's Surface: Recent Advances, Springer-Verlag Berlin Heidelberg, XXXIII, 517 pp., 2008.

Barnston, A. G. and Livezey, R. E.: Classification, seasonality and persistence of low-frequency atmospheric circulation patterns, Mon. Weather Rev., 115, 1083–1126, 1987.

Budyko, M. I.: The heat balance of the earth's surface/transl. from the Russ. N.A. Stepanova, Washington, US Dept. of Commerce, Weather Bureau, 259 pp., 1958.

Beyrich, F. and Mengelkamp, H.-T.: Evaporation over heterogeneous land surface: EVA-CRIPS and the LITFASS-2003 experiment, Bound.-Lay. Meteorol., 121(1), 5–32, 2006.

Beyrich, F., Leps, J. P., Mauder, M., Bange, J., Foken, T., Huneke, S., Lohse, H., Lüdi, A., Meijninger, W. M. L., Mironov, U. W., and Zittel, P.: Are-averaged surface fluxes over the litfass region based on eddy-covariance measurements, Bound.-Lay. Meteorol., 121(1), 33–65, 2006.

Chernokulsky, A. V. and Mokhov, I. I.: Intercomparison of Global and Zonal Cloudiness Characteristics from Different Satellite and Ground Based Data, Issledovanie Zemli iz kosmosa, 3, 12–29, 2010.

Da Silva, A. M., Young, C. C., and Levitus, S.: Atlas of Surface Marine Data, Algorithms and Procedures, NOAA Atlas NESDIS 6, US Dep. of Commer., Natl. Oceanic and Atmos. Admin./Natl. Environ. Satellite Data Inf. Serv., Silver Spring, Md., vol. 1, 1994.

Eliseev, A. A., Privalov, V. I., Paramonova, N. N., and Utina, Z. M.: Experimental Study id Heat-Flux Divergences in the Atmospheric Surface Layer, Izvestiya, Atmos. Ocean. Phys., 38(5), 649–657, 2002.

Foken, T.: The energy balance closure problem – An overview, Ecol. Appl., 18, 1351–1367, 2008.

Gupta, S. K., Ritchey, N. A., Wilber, A. C., Whitlock, C. H., Gibson, G. G., and Stackhouse, P. W.: A climatology of surface radiation budget derived from satellite data, J. Climate, 12, 2691–2710, 1999.

BGD

8, 4331–4357, 2011

Heinemann, G. and Kerschgens, M.: Comparison of methods for area-averaging surface energy fluxes over heterogeneous land surfaces using high-resolution non-hydrostatic simulations, Int. J. Climatol., 25, 379–403, 2005.
Heinemann, G. and Kerschgens, M.: Simulation of surface energy fluxes using high-resolution non-hydrostatic simulations and comparisons with measurements for the LITFASS-2003 experiment, Bound.-Lay. Meteorol., 121(1), 195–220, 2006.
Heret, C., Tittebrand, A., and Berger, F. H.: Latent heat fluxes simulated with a non-hydrostatic weather forecast model using actual surface properties from measurements and remote sensing, Bound.-Lay. Meteorol., 121(1), 175–194, 2006.
Jimener, C., Prigent, C., and Aires, F.: Toward am estimation of global land surface heat fluxes from multisatellite observations, J. Geophys. Res., 114(6), 1–22, D06305, 2009.
Ippolitov, I. I., Kabanov, M. V., Loginov, S. V., and Kharyutkina, E. V.: Structure and Dynamic of Meteorological Fields on the Asian Region of Russia in the Period of the Global Warming for 1975–2005, Journal of Siberian Federal University – Biology, 4(1), 323–344, 2008.
Ippolitov, I. I., Loginov, S. V., and Sevastyanov, V. V.: Comparative analysis of total radiation in West Siberia by Reanalysis data and network observations, Atmospheric and Oceanic Optics, 22(1), 34–37, 2009.
Khlebnikova, E. I. and Sall, I. A.: Peculiarities of climatic changes in cloud cover over the Russian Federation, Russ. Meteorol. Hydrol., 34(7), 411–417, 2009.
Liu, J., Curry, J. A., Rossow, W. B., Key, J. R., and Wang, X.: Comparison of surface radiative flux data over the Arctic Ocean, J. Geophys. Res., 110(2), C02015, doi:10.1029/2004JC002381, 2005.
Meleshko, V. P. (Ed.): Assesment report on climate change and its consequences in Russian Federation Climate Change, Federal Service for Hydrometeorology and Environmental Monitoring (ROSHYDROMET), 1, 227 pp., 2008.
Pavlov, A. V.: Calculation and Regulation of the Cryotic Regime of Soil, Novosibirsk: Nauka, 240 pp., 1980.
Rossow, W. and Zhang, Y.: Calculation of surface and top of atmosphere radiative fluxes from physical quantities based on ISCCP data set 2: Validation and first results, J. Geophys. Res., 100, 1167–1197, 1995.
Serreze, M. C., Barrett, A. P., Slater, A. G., Steele, M., Zhang, J., and Trenberth, K. E.: The large-scale energy budget of the Arctic, J. Geophys. Res., 112, D11122, doi:10.1029/2006JD008230, 2007.

BGD
8, 4331–4357, 2011

Smith, G. L., Wilber, A. C., Gupta, S. K., and Stackhouse, P. W.: Surface radiation budget and climate classification, J. Climate, 15, 1175–1188, 2002.

Solomon, S., Qin, D., Manning, M., Chen, Z., Marquis, M., Averyt, K. B., Tignor, M., and Miller, H. L. (Eds.): Climate Change. The Physical Science Basis. Contribution of Working Group I to the Fourth Assessment Report of the Intergovernmental Panel on Climate Change, Cambridge University Press, Cambridge, United Kingdom and New York, NY, USA, 996 pp., 2007.

Trenberth, K. E. and Solomon, A.: The global heat balance: Heat transports in the atmosphere and ocean, Clim. Dynan., 10, 107–134, 1994.

Trenberth, K. E. and Stepaniak, D. P.: The flow of energy through the Earth's climate system. Q. J. Roy. Meteor. Soc., 130, 2677–2701, 2004.

Wilber, A. C., Smith, G. L., Gupta, S. K., and Stackhouse, P. W.: Annual cycles of surface shortwave radiative fluxes, J. Climate, 19, 535–547, 2006.

Zhang, Y.-C. and Stackhouse Jr., P. W.: Comparison of different global information sources used in surface radiative flux calculation: Radiative properties of the near-surface atmosphere, J. Geophys. Res., 111, D13106, doi:10.1029/2005JD006873, 2006.

Zhang, Y.-C., Lacis, A. A., Oinas, V., and Mishchenko, M. I.: Calculation of radiative fluxes from the surfaceto top of atmosphere based on ISCCP and otherglobal data sets: Refinements of the radiative transfermodel and the input data, J. Geophys. Res., 109, D19105, doi:10.1029/2003JD004457, 2004.

Zhang, Y.-C., Romanou, A., and Wielicki, B. A.: Decadal variations of global energy and ocean heat budget and meridional energy transports inferred from recent global data sets, J. Geophys. Res., 112, D22101, doi:10.1029/2007JD008435, 2007.

BGD
8, 4331–4357, 2011

Table 1. Air surface temperature for ATR.

Month	By stations (1976–2005)		JRA-25 (1979–2008)	
	$\overline{T}$, °C	$\overline{T_{tr}}$, °C/decade	$\overline{T}$, °C	$\overline{T_{tr}}$, °C/decade
Jan	−27.9	0.27	−21.6	0.91
Feb	−24.7	0.51	−18.8	0.4
Mar	−15.9	0.65	−12.2	0.98
Apr	−5.2	0.23	−3.5	0.55
May	4.5	0.55	6.0	0.63
Jun	13.0	0.37	14.9	0.52
Jul	16.3	0.46	18.0	0.34
Aug	13.0	0.26	14.2	0.28
Sep	5.4	0.19	6.8	0.14
Oct	−5.5	0.57	−3.2	0.48
Nov	−18.5	0.29	−13.9	0.65
Dec	−26.3	−0.03	−19.6	−0.09
Year	−6.4	0.34	−2.7	0.48

BGD
8, 4331–4357, 2011

Table 2. Variability of monthly averaged values of TC, $Q_{\downarrow S}$, LE and P over ATR.

Month	Downward Solar Radiation		Total Cloudiness		Latent Energy LE		Sensible Energy P	
	$\overline{Q_{\downarrow S}}$, W m^{-2}	$\overline{Q_{\downarrow S\,tr}}$, W m^{-2}/decade	$\overline{TC}$, %	$\overline{TC_{tr}}$, %/decade	$\overline{LE}$, W m^{-2}	$\overline{LE_{tr}}$, W m^{-2}/decade	$\overline{P}$, W^{-2}	$\overline{P_{tr}}$, W m^{-2}/decade
Jan	13.7	−0.04	58	−0.17	0.1	−0.12	−23.0	−0.62
Feb	48.4	−0.02	56	−0.01	1.0	0.06	−17.5	−0.42
Mar	116.6	−1.24	53	0.04	4.6	0.48	−6.8	−1.22
Apr	198.9	−0.70	49	−0.07	16.8	0.23	17.7	−0.59
May	252.9	−1.85	48	−0.06	40.0	0.47	39.3	−2.56
Jun	269.5	−1.79	46	0.03	58.1	0.36	46.4	−1.87
Jul	248.2	0.38	45	−0.03	62.9	0.71	39.9	−0.70
Aug	186.1	−1.02	50	0.04	45.1	−0.03	25.3	−0.39
Sep	115.5	−1.00	55	0.04	25.9	0.25	7.8	−0.69
Oct	57.8	−0.48	60	0.05	10.4	−0.14	−11.4	−0.88
Nov	20.4	−0.18	62	−0.07	2.3	−0.1	−21.0	−0.03
Dec	7.0	−0.03	59	−0.12	0.4	−0.1	−23.8	0.13

BGD
8, 4331–4357, 2011

Table 3. Annual variation of R^2.

Month	Clear sky		With cloudiness	
	$\overline{R^2}$	σ_{R^2}	$\overline{R^2}$	σ_{R^2}
Jan	0.71	0.26	0.80	0.23
Feb	0.58	0.23	0.73	0.20
Mar	0.49	0.22	0.57	0.20
Apr	0.49	0.19	0.56	0.18
May	0.48	0.18	0.53	0.17
Jun	0.68	0.24	0.70	0.20
Jul	0.71	0.12	0.74	0.10
Aug	0.65	0.16	0.72	0.13
Sep	0.49	0.16	0.59	0.14
Oct	0.47	0.20	0.54	0.21
Nov	0.64	0.22	0.75	0.16
Dec	0.57	0.26	0.72	0.23

BGD
8, 4331–4357, 2011

Table 4. Estimations of predictors' contribution.

Month	δQ_n	δE_{eff}	δE_{g}	δTC
Jan	26.8	37.2	20.2	15.8
Feb	20.0	41.3	21.5	17.3
Mar	21.5	42.1	15.3	21.1
Apr	50.6	14.9	6.4	28.1
May	53.8	17.9	6.5	21.8
Jun	43.8	32.0	10.8	13.4
Jul	45.3	23.3	15.5	15.9
Aug	39.7	30.4	19.0	10.9
Sep	35.0	36.4	14.1	14.5
Oct	20.2	31.6	17.2	31.1
Nov	7.3	35.9	24.4	32.4
Dec	19.5	36.8	25.7	18.0

BGD
8, 4331–4357, 2011

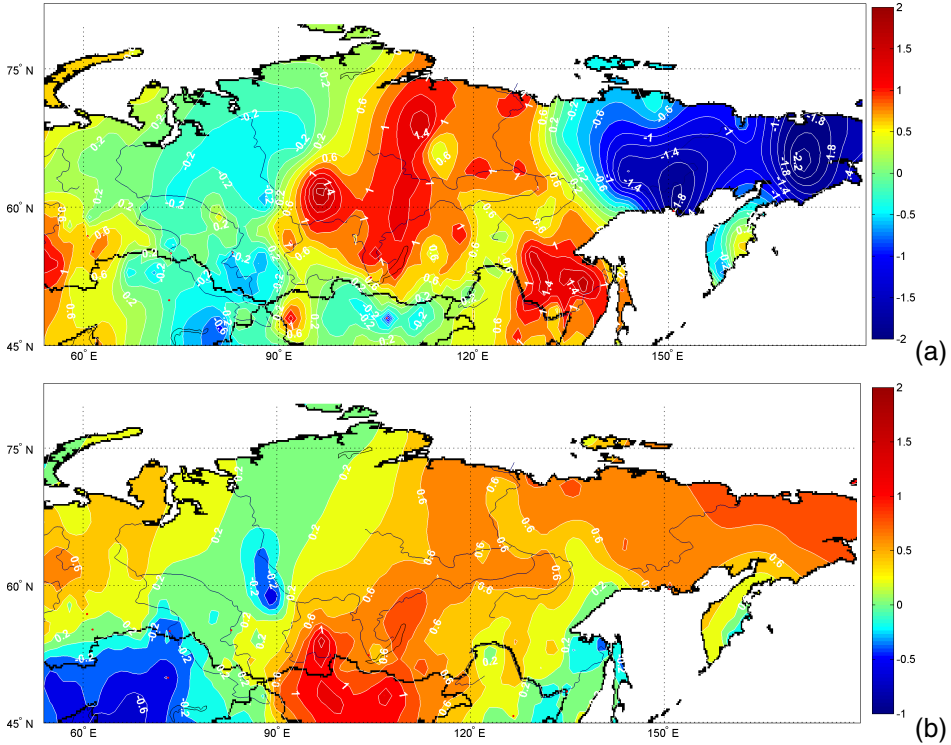

Fig. 1. The spatial distribution of temperature trend values (°C/decade) over ATR for January **(a)** and July **(b)** by observational data.

BGD
8, 4331–4357, 2011

Variability of radiative balance elements and air temperature

E. V. Kharyutkina et al.

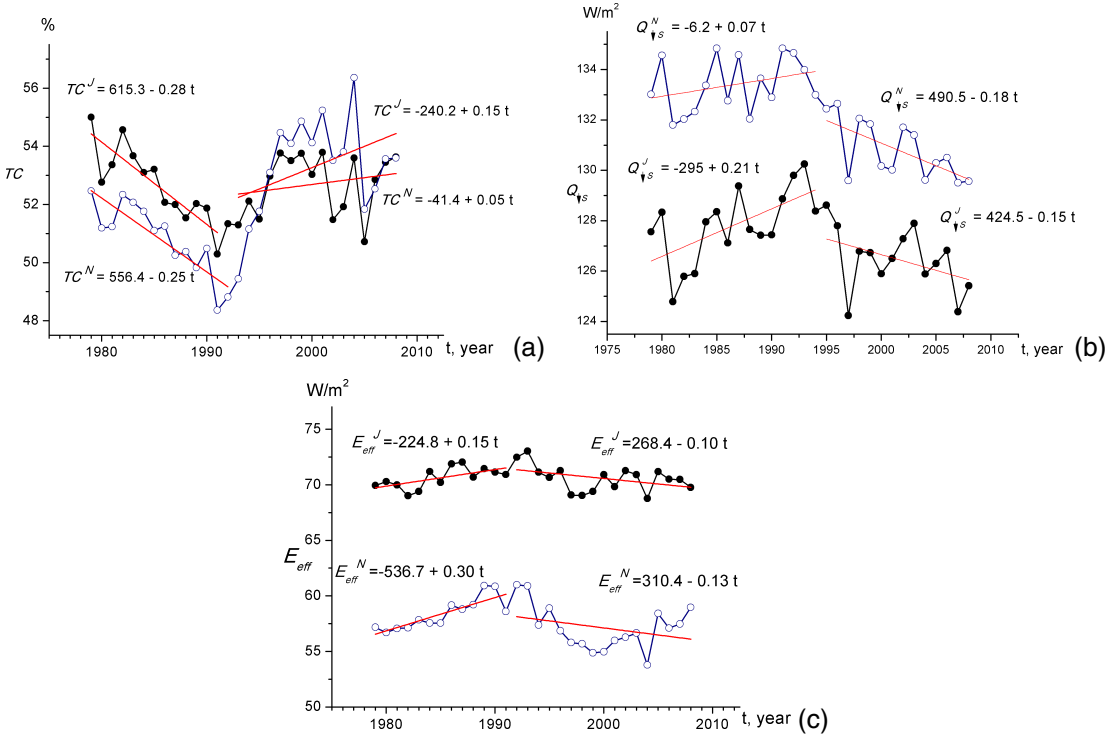

Fig. 2. The temporal variability of total cloud cover (TC) **(a)**, downward short-wave radiation at the surface $Q_{\downarrow S}$ **(b)** and effective radiation E_{eff} **(c)** over ATR by JRA-25.

BGD
8, 4331–4357, 2011

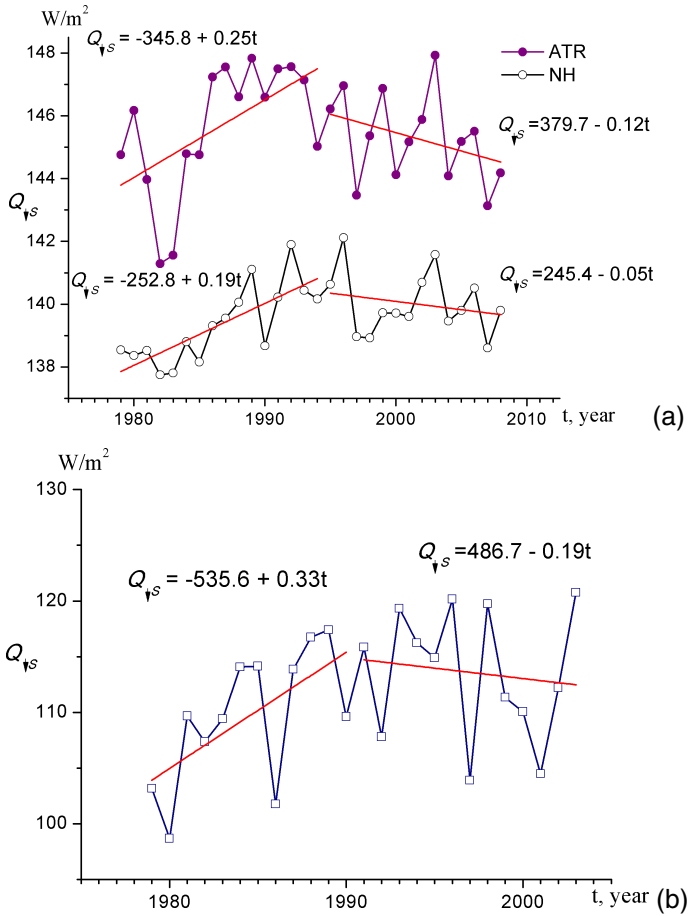

Fig. 3. The temporal variability of downward short-wave radiation at the surface $Q_{\downarrow S}$ by JRA-25: over ATR and Northern Hemisphere **(a)** and at Aleksandrovskoe station (60°26′ N, 77°52′ E) **(b)**.

BGD
8, 4331–4357, 2011

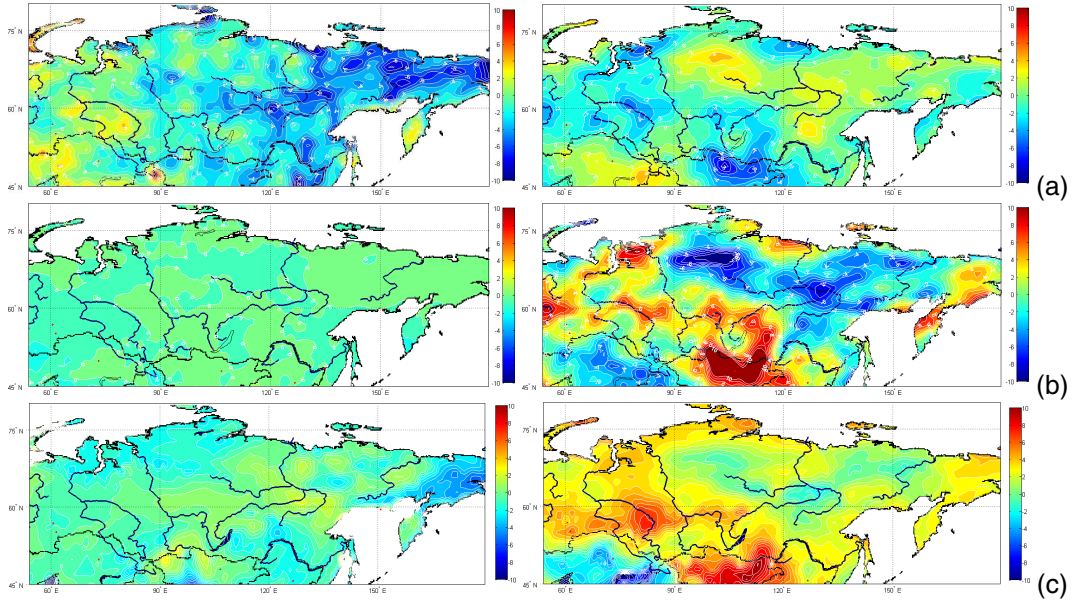

Fig. 4. The spatial variability of total cloud cover trend (TC, %/decade) **(a)**, downward shortwave radiation trend at the surface ($Q_{\downarrow S}$, W m^{-2}/decade) **(b)** and effective radiation trend (E_{eff}, W m^{-2}/decade) **(c)** over ATR for January (left) and July (right) by JRA-25.

BGD
8, 4331–4357, 2011

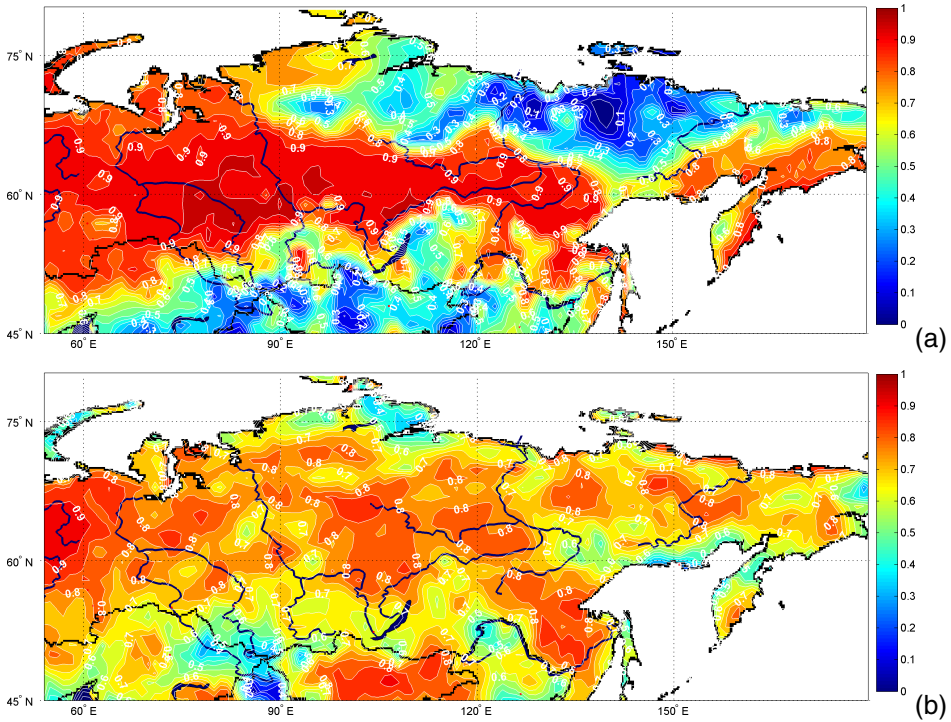

Fig. 5. The spatial distribution of determination coefficient by Eq. (3) for January **(a)** and July **(b)**.

BGD
8, 4331–4357, 2011

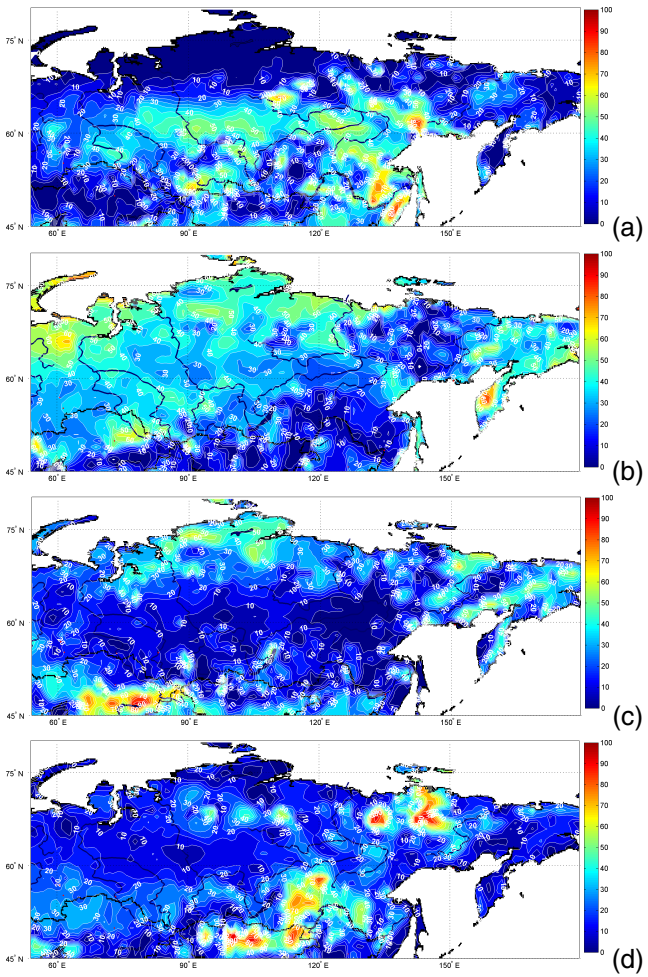

Fig. 6. Spatial distribution of predictors in January: **(a)** δQ_n, **(b)** δE_{eff}, **(c)** δE_{g}, **(d)** δTC.

BGD
8, 4331–4357, 2011

Variability of radiative balance elements and air temperature

E. V. Kharyutkina et al.